Modest increase in the de novo single nucleotide mutation rate in house mice born by assisted reproduction

Laura Blanco-Berdugo, Alexis Garretson and Beth L Dumont

Genome Res. published online November 13, 2025
Access the most recent version at doi:10.1101/gr.281180.125

Modest increase in the *de novo* single nucleotide mutation rate in house mice born by assisted reproduction

Laura Blanco-Berdugo[1] Alexis Garretson[1,2], and Beth L. Dumont[1,2,3,*]

1. The Jackson Laboratory, 600 Main Street, Bar Harbor ME 04609
2. Tufts University, Graduate School of Biomedical Sciences, 136 Harrison Ave, Boston MA 02111
3. Graduate School of Biomedical Science and Engineering, The University of Maine, Orono, Maine, USA 04469

* **Address for Correspondence**:
Beth Dumont
The Jackson Laboratory
600 Main Street
Bar Harbor, ME 04609

P: 207-288-6647
E: beth.dumont@jax.org

Running Title: ART increases mutation rate in mice

Key words: Assisted Reproductive Technology, in vitro fertilization, mutation rate, house mouse, mutation spectrum

ABSTRACT

Approximately 2.6% of live births in the United States are conceived using assisted reproductive technologies (ART). While some ART, including in vitro fertilization (IVF) and intracytoplasmic sperm injection, are known to alter the epigenetic landscape of early embryonic development, their impact on DNA sequence stability is unclear. Here, we leverage the strengths of the laboratory mouse model system to investigate whether a standard ART series (ovarian hyperstimulation, gamete isolation, IVF, embryo culture, and embryo transfer) affects genome stability. Age-matched cohorts of 12 ART-derived and 16 naturally conceived C57BL/6J inbred mice were reared in a controlled setting and whole-genome sequenced to ~50× coverage. Using a rigorous pipeline for de novo single nucleotide variant (dnSNV) discovery, we observe a ~30% (95% CI: 4.5% - 56%) increase in the dnSNV rate in ART compared to naturally conceived mice (P = 0.017). Analysis of the dnSNV mutation spectrum identified signatures attributable to germline DNA repair activity but revealed no differentially enriched signatures between cohorts. We observe no enrichment of dnSNVs in specific genomic contexts, suggesting that the observed rate increase in ART-derived mice is a general genome-wide phenomenon. Together, our findings show that ART is moderately mutagenic in house mice and motivate future work to define the procedure(s) associated with this increased mutational vulnerability. While we caution that our findings cannot be immediately translated to humans, they nonetheless emphasize a pressing need for investigations on the potential mutagenicity of ART in our species.

INTRODUCTION

Worldwide, approximately 1,000,000 babies are born by assisted reproductive technologies (ART) each year (ESHRE Factsheet on ART), accounting for over 2.5% of live births in the United States (CDC 2024b) and many other Western countries (Smeenk et al. 2023; Katagiri et al. 2023). This number has risen steadily over the last decade (CDC 2024a) and is projected to grow further due to rising infertility rates (Nugent and Chandra 2024) and delayed reproduction (Osterman et al. 2025). The human health consequences of the increased reliance on ART are potentially substantial. Prior work has shown that various ART procedures are associated with altered methylation patterns in both model organisms (de Waal et al. 2015; Koustas and Sjoblom 2016; Yu et al. 2019; Ooga et al. 2023) and humans (Barberet et al. 2021; Choux et al. 2018; Ghosh et al. 2017; Mani et al. 2019; Håberg et al. 2022; Song et al. 2015), with downstream consequences for the expression of key genes required for totipotency and early development (Rivera et al. 2008; Giritharan et al. 2007; Hayashi 2003; Kohda 2013; Tan et al. 2016). These molecular changes are associated with increased rates of imprinting-related disorders (Cortessis et al. 2018; Hattori et al. 2019), and may contribute to higher rates of adverse pregnancy, perinatal, neonatal, and long-term health outcomes in ART-derived offspring (McDonald et al. 2009; Palomba et al. 2016; Luke et al. 2021; Hart and Wijs 2022; Zhang et al. 2025).

While it is well-established that various ART procedures can perturb the dynamics of epigenetic reprogramming in the pre-implantation embryo and developing fetus (Mani et al. 2019), it is not clear whether ART influences the integrity and stable transmission of the underlying DNA sequence itself. Prior investigations exploring this possibility have yielded contradictory findings. Some studies have concluded that ART is associated with an increased burden of structural mutations and aneuploidies (Bean 2002; Bonduelle 2002; Lee et al. 2023), while other studies have reported no significant increase in large-scale structural rearrangements in ART compared

to naturally-conceived offspring (Zamani Esteki et al. 2019). Similarly, whereas a prior study in mice found no evidence for an increased point mutation rate in animals born via in vitro fertilization (IVF) (Caperton et al. 2007), a retrospective comparative analysis in humans uncovered a significantly higher de novo point mutation rate in IVF-born children (Wang et al. 2021). However, the underlying etiology of subfertility or infertility may predispose patients seeking ART to elevated rates of germline genome instability (Ruth et al. 2021), and any observed increase in the mutation burden associated with ART could be due to ascertainment bias.

Despite conflicting earlier findings, there are compelling lines of evidence to support the hypothesis that ART procedures may be intrinsically mutagenic. First, epigenetic features, including methylation at CpG dinucleotides and H3K9me3 marks, directly shape local mutation rates (Makova and Hardison 2015; Chen et al. 2017). Thus, the genome-wide epigenetic dysregulation observed in ART-derived embryos could secondarily alter the genomic distribution and rate of new mutations compared to naturally conceived embryos (Mani et al. 2019). Second, the first few embryonic cell divisions are especially error-prone and uniquely vulnerable to the accumulation of large-scale structural mutations and aneuploidies (Vanneste et al. 2009; Currie et al. 2022). Exposure to stressors unique to the in vitro environment may exacerbate genomic instability at this critical time point in early development. In particular, ART-derived embryos are often cultured at oxygen levels that do not precisely replicate those encountered in the maternal reproductive tract (Konstantogianni et al. 2024); exposure to either hyperoxic or hypoxic culture conditions can promote DNA damage and genomic instability (Gille et al. 1994; Bristow and Hill 2008). Additionally, compounds such as glucocorticoids present in gamete and IVF culture media could perturb the early epigenetic landscape of the developing embryo, leading to widespread regulatory and metabolic changes with downstream implications for genome integrity (Zhao et al. 2022).

Here, we harness the efficiency of ART in the laboratory mouse to rigorously test whether a standard regimen of ART procedures consisting of (1) ovarian hyperstimulation via administration of exogenous hormones, (2) gamete isolation and culture, (3) *in vitro* fertilization (IVF), (4) embryo culture, and (5) embryo transplantation into a receptive uterus influences the stable transmission of the mammalian genome. We use whole-genome sequencing to identify *de novo* mutations in cohorts of age-matched ART-derived and naturally conceived mice. Our reliance on mice of a single inbred strain background allows us to rigorously control for potential genetic influences and environmental exposures on mutation rates, eliminating these confounding factors from our analysis and overcoming a major limitation of retrospective clinical studies. Our study presents the first direct experimental test of the hypothesis that ART impact genome integrity in a rigorously controlled in vivo mammalian model system.

RESULTS

De novo single nucleotide variant discovery in natural and ART-conceived mice

We aimed to test whether a standard ART protocol influences the overall incidence of dnSNVs arising in gametes and/or during early embryonic development in a mouse model. Specifically, we focus on the sequential procedures of ovarian hyperstimulation by exogenous hormone injection, oocyte collection, sperm isolation, gamete culture, *in vitro* fertilization, embryo culture to the 2-cell stage (~1 day post fertilization), and fresh embryo transfer to a pseudo-pregnant host dam. This series of ART procedures is routinely employed in the course of mouse husbandry for strain rederivation and colony expansion, and parallels protocols used in human fertility clinics, with some exceptions. Notably, human fertility clinics typically employ intracytoplasmic sperm injection (ICSI) to achieve fertilization, bypassing the natural requirements for sperm motility and functional gamete interaction. Additionally, human embryos are typically cultured to the blastocyst stage (~5 days post fertilization) and, in most cases, undergo a freeze-thaw cycle prior to transfer.

We generated age-matched cohorts of natural- and ART-derived C57BL/6J mice from a common G0 founder pair **(Figure 1A).** Two G1 females were mated to a single male sibling, yielding two litters of naturally conceived mice. To obtain a matched ART-derived cohort, oocytes from two hormonally super-ovulated G1 female siblings were harvested and *in vitro* fertilized with sperm from a second G1 male littermate. Two-cell embryos derived from each of the two females were then transferred to two pseudo-pregnant C57BL/6J recipient dams and reared to term. A total of 16 natural-born and 12 ART-conceived G2 progeny were whole-genome sequenced to ~50-72× coverage using two independent sequencing libraries (**Supplemental Table 1; Supplemental Figure 1**). The six G1 parents and two G0 pedigree founders were additionally sequenced to enable discrimination between dnSNVs and segregating variants within our pedigree (>75× coverage; two libraries per sample;

Supplemental Table 1; **Supplemental Figure 2**). By bottlenecking the breeders used in this experiment through a single G0 founder pair and using a common sire for each treatment group, we minimize the number of background segregating mutations present in our G2 cohorts, limiting this potential source of false positive dnSNVs. Simulations based on empirical coverage estimates indicate that our study design has 80% power to detect a ~35% increase in the dnSNV rate between the ART and naturally conceived cohorts, assuming a baseline mutation rate equivalent to that previously reported for C57BL/6J mice (Lindsay et al. 2019) (**Supplemental Figure 3**).

Sequencing reads from each sample were aligned to the GRCm39 mouse reference genome, followed by SNV calling, dnSNV identification, and application of a post hoc filtering pipeline informed by tailored simulations (Garretson et al. 2025) (see **Methods**). Our strategic use of the reference strain, C57BL/6J, effectively eliminates reference genome biases to maximize the accuracy of SNV calling and dnSNV discovery. On average, we identified 17.3 high-confidence autosomal dnSNVs in samples from the natural mating cohort (range = 11-25), corresponding to an estimated per base mutation rate of 3.88×10^{-9} per generation (per sample range: 2.47×10^{-9} – 5.61×10^{-9}). This mutation rate estimate is in agreement with previously reported mutation rates for house mice (~$3.5–8.0 \times 10^{-9}$ per site per generation) (Uchimura et al. 2015; Lindsay et al. 2019; Bergeron et al. 2023; López-Cortegano et al. 2025). In contrast, offspring generated via ART exhibit a significantly elevated dnSNV burden, with an average of 22.1 autosomal dnSNVs per individual and a dnSNV mutation rate of 4.96×10^{-9} (range: 13–34; range of mutation rate per sample: 2.91×10^{-9} to 7.62×10^{-9}; Negative Binomial Regression, Incidence Rate Ratio (IRR) with natural cohort as baseline =1.276, 95% CI = 1.045-1.558, *P*-value = 0.017**; Figure 1B**). A more complex model including sex and sex × cohort interaction terms revealed no significant sex or interaction effects, suggesting that the elevated mutation burden associated with ART is not restricted to a single sex (**Figure 1B**; $P > 0.3$).

Our finding of a significant increase in dnSNVs in ART-derived samples suggests that the tested ART protocol adversely impacts genome stability in gametes, zygotes, or early-stage embryos. However, systematic differences in sequencing data quality could also lead to differences in the number of false-positive or false-negative dnSNV calls between cohorts. Importantly, sequencing data quality is universally high across our G2 samples (**Supplemental Figure 1**), dnSNV calls are supported by similar variant quality metrics in both cohorts (**Supplemental Figure 4**), and our findings are recapitulated using sequencing data from replicate libraries from each sample (see Methods; **Supplemental Tables 3 and 4; Supplemental Figure 5**). We conclude that the observed differences in mutation burden between ART- and naturally-conceived offspring cannot be explained by cohort-specific technical artifacts.

No difference in mutation spectra between naturally conceived and ART-derived mice

Exposure to specific environmental mutagens can alter the spectrum of mutations that accumulate in somatic tissues (Pleasance et al. 2010; Alexandrov et al. 2020), prompting us to ask whether the altered hormonal milieu and *in vitro* environment encountered during the generation of ART-born mice modifies the prevalence of specific types of mutations compared to those recovered in naturally-conceived animals. Both breeding cohorts exhibit qualitatively similar transition and transversion fractions (Two-tailed Wilcoxon rank-sum test; $P > 0.7$; **Figure 1C**), with estimates closely approximating those from prior studies of germline mutations in house mice (Lindsay et al. 2019; López-Cortegano et al. 2024). Furthermore, the two cohorts show no difference in the relative frequency of individual mutation types (Two-tailed Wilcoxon rank-sum test, $P > 0.1$) or the overall single-base mutation spectrum (G-test, $P > 0.05$; **Figure 1D**).

We further partitioned dnSNVs by flanking nucleotide context and assigned spectra to known mutation signatures (Alexandrov et al. 2020). The resulting trinucleotide mutation count matrix is sparse, with 7 of 96 mutation classes with no observable dnSNVs in either cohort, and 28

mutation classes featuring dnSNVs in only one cohort. Nonetheless, dnSNVs across both cohorts exhibit patterns attributable to mutation signatures associated with germline DNA repair activity (SBS5 and SBS30; **Figure 2A**), consistent with expectations for our data. We find no significant cohort-level differences in the proportions of dnSNVs ascribable to defined mutational signatures (**Figure 2A**), although ART samples exhibit a significant increase in the C[C>A]A trinucleotide mutation fraction compared to natural-born samples (modified Chi-square, P = 0.019, **Figure 2B**). Taken together, these findings reveal broad similarities in the mutation spectrum between ART-derived and natural-born mice, with the caveat that our analysis is likely underpowered to detect subtle or moderate cohort differences.

Evaluating the genomic landscape of dnSNVs in natural-born and ART-derived mice

We next examined whether the distribution of new mutations differs between our two cohorts with respect to various genomic features, including GC content, functional annotations, and repetitive elements. dnSNVs ascertained in both cohorts are uniformly distributed across the genome (Poisson test applied to mutation counts in 10Mb bins, $P > 0.3$; **Supplemental Figure 6A**) and arise in regions of similar GC content (Two-tailed Wilcoxon rank-sum test, P = 0.215 **Supplemental Figure 6B**). Likewise, we detect no significant enrichment or depletion of ART-associated dnSNVs in CpG islands (Fisher's exact test, P = 0.686; **Supplemental Figure 6C**). The majority of dnSNVs occur in intronic and distal intergenic regions (**Figure 3A**), with no cohort differences in the distribution of dnSNVs across different genomic annotations (Two-tailed Wilcoxon rank-sum test, $P > 0.05$; **Figure 3**). Similarly, there is no difference in the predicted variant effects of new mutations between natural- and ART-born mice (**Figure 3B**). The number of dnSNVs in ART-derived mice is modestly increased within LINEs, but the difference does not reach statistical significance after applying a multiple test correction (Fisher's exact test, Bonferroni-corrected $P > 0.05$; **Figure 3C**). Despite an overall increase in

dnSNV rate in ART-derived mice, the genomic landscape of dnSNVs is largely indistinguishable between breeding cohorts.

Contrasting the epigenomic and genome regulatory context of dnSNVs

Early development involves the coordinated erasure, deposition, and redistribution of numerous DNA and histone modifications (Reik et al. 2001). Prior work has established that this epigenetic reprogramming is perturbed under in vitro conditions relative to in vivo (Håberg et al. 2022). Given that diverse chromatin modifications are associated with intragenomic mutation rate variation (Makova and Hardison 2015), we next examined whether dnSNVs arise in distinct epigenetic contexts in our two cohorts. We intersected dnSNV positions from both cohorts with genome-wide maps of histone modifications in mouse embryonic stem cells (mESCs) (Yue et al. 2014) and early mouse embryos (Liu et al. 2016). There is no cohort-level difference in the proportion of dnSNVs that arise in regions associated with H3K27ac, H3K36me3, H3K4me1, H3K4me3, H3K9ac, or H3K9me3 histone modifications in either mESCs or mouse embryos (Fisher's exact tests, $P > 0.25$; **Supplemental Figures 7, 8**).

In somatic cells, transcription-coupled repair reduces dnSNV rates in highly expressed genes compared to more lowly expressed or transcriptionally silenced genes (Moore et al. 2021). Although gene expression differences have been documented between ART-derived and natural-born progeny (Song et al. 2015), we find no cohort-level difference in the transcriptional activity of genes neighboring dnSNVs in C57BL/6J-derived mESCs (Two-tailed Wilcoxon rank-sum test, $P = 0.89$; **Supplemental Figure 9**).

Most dnSNVs are thought to arise from errors in DNA replication, with later-replicating regions of the genome exhibiting elevated mutation rates compared to early-replicating regions (Stamatoyannopoulos et al. 2009). Using published replication timing profiles from mESCs, we replicate this prior result, confirming that dnSNVs aggregated across both cohorts are enriched

in late-replicating regions (Two-tailed Wilcoxon rank-sum test, $P < 10^{-2}$; **Supplemental Figure 10A,B**). However, we find no evidence of differences in overall replication timing at dnSNV sites between cohorts (Two-tailed Wilcoxon rank-sum test, $P > 0.5$; **Supplemental Figure 10C,D**) (Pratto et al. 2021; Dey et al. 2015).

No difference in the developmental timing of dnSNVs between ART-derived and naturally-conceived mice

The excess dnSNVs recovered in our ART-derived mice may have originated during (i) gamete formation in vivo, (ii) in vitro gamete manipulation and culture, (iii) the transition from zygote to 2-cell stage, or (iv) later stages of embryonic development, resulting in somatic mosaicism. We profiled the allele-depth ratio (i.e., the proportion of sequencing reads supporting the alternative allele) across all dnSNVs to assess the developmental timing of mutations in our two cohorts. dnSNVs that arise in parental gametes will be constitutively present in the genome of offspring and will appear with an allele-depth ratio of approximately 0.5, whereas mutations that arise during the zygote to 2-cell transition will have an allele-depth ratio ~0.25. Mutations arising later in development will exhibit lower allele depth ratios and are unlikely to be detected given our sequencing depth (~50×) and reliance on a single tissue type. We observed no significant difference in the distribution of allele-depth ratios for dnSNVs between animals conceived via ART and those conceived naturally (Two-tailed Wilcoxon rank-sum test, $P = 0.29$; **Supplemental Figure 11**), indicating no evidence of differences in the developmental origin of dnSNVs between cohorts.

No detectable difference in de novo structural variation rates between ART-derived and natural-born mice

The rate of *de novo* SV is predicted to be at least one order of magnitude lower than the single-nucleotide mutation rate (Belyeu et al. 2021a), a consideration that limits our power to detect small or modest differences in SV mutation rate (**Supplemental Figure 3**). However, a recent

report identified a ~5-fold increase in the rate of de novo structural variants (SVs) in cattle born via ART compared to naturally conceived animals (Lee et al. 2023), motivating efforts to quantify de novo SV rates in our cohorts. We utilized an ensemble SV calling approach to identify de novo deletions and duplications >50 bp in G2 samples (see **Methods**). We identified eight high-confidence germline de novo SVs (4 deletions and 4 duplications) in natural-born samples and seven (4 deletions and 3 duplications) in ART-derived samples—an insignificant difference (ART cohort as baseline, IRR = 1.14, 95% CI: 0.41 – 3.19, *P* = 0.796; **Supplemental Table 5**). Approximately half of these SV calls localize to a cluster of C2H2 KRAB zinc finger proteins on distal Chromosome 4 (145.3 Mb), a locus recently shown to be highly copy number variable in house mice (Bruno et al. 2025). SVs at this genomic position include reciprocal ~2.3Mb duplications and deletions, with both duplication and deletion alleles present in samples from the ART-derived and natural-born cohorts. While these patterns could suggest germline mosaicism in the G0 founders that escaped detection in our G1 mice or extreme instability of this locus, we think it most likely that these calls are artifacts caused reference assembly errors at this locus (Bruno et al. 2025). Our findings underscore the challenges and limitations of SV calling in short read data and motivate the future adoption of long-read sequencing technologies to enable accurate discovery of de novo SVs in this experimental paradigm.

DISCUSSION

Prior work has shown that ART is associated with epigenetic and transcriptomic changes in early embryos, but the potential impact of ART procedures on DNA sequence integrity is not well understood. Here, we took advantage of a carefully controlled mouse model system to directly estimate the burden of dnSNVs in C57BL/6J inbred mouse cohorts conceived through a standardized ART protocol or via natural mating. We document a statistically significant increase in the overall dnSNV rate in ART-derived mice compared to their age- and genetically-matched natural-born counterparts. Our dnSNV discovery pipeline surpasses field standards for rigor, relying on two independent sequencing libraries for each sample and using a simulation-informed protocol for dnSNV discovery in inbred mouse genomes (Garretson et al. 2025).

The biological mechanisms underlying the elevated rate of dnSNVs in ART-derived mice remain unclear. Known mutational processes often leave distinct genomic signatures, including signatures attributable to oncogenic processes (Alexandrov et al. 2020) and germline DNA repair mechanisms (Garcia-Salinas et al. 2025). While the modest number of dnSNVs identified may obscure subtle differences in the mutational landscape, we find no differential enrichment of mutation signatures in our ART-derived and natural-born cohorts. Further, we find no differences in the transition/transversion ratio, the mutation spectrum, or the genomic distribution of dnSNVs between cohorts. Similarly, we observe no differential enrichment of dnSNVs across various epigenetic contexts or with respect to GC content, local transcriptional activity, or replication timing.

Future studies will be necessary to determine whether the elevated mutation burden observed in ART-derived mice arises from a specific step in our ART protocol or reflects the cumulative effects of multiple procedures. One plausible contributor is ovarian stimulation using exogenous follicle-stimulating hormone and human chorionic gonadotropin. These hormones induce the

resumption of meiosis in oocytes, a process known to be highly error-prone (Hassold and Hunt 2001). Indeed, there is some empirical support that hormone-induced ovulation is mutagenic. Ovulation induction has been associated with elevated risks of miscarriage and congenital anomalies in humans (Hansen et al. 2013; Davies et al. 2012), and a recent retrospective analysis suggested a link between this intervention and increased maternally transmitted mutations (Wang et al. 2021). Additionally, there is growing evidence linking ovulation induction with transcriptional and epigenetic alterations to oocytes (Market-Velker et al. 2009; Lopes et al. 2002; Xie et al. 2024), including changes in the expression of genes implicated in DNA damage repair (Daugelaite et al. 2023). Nonetheless, we cannot exclude the potential influence of other ART-related factors, such as mechanical stress during embryo manipulation or the physicochemical properties of the *in vitro* culture environment. Our use of male and female parents from a single inbred strain limits the ability to assign the parental origin of the dnSNVs reported here, an advantage that could help future studies pinpoint the source of the excess dnSNV burden associated with ART.

Overall, the ~30% mutation rate increase observed in ART-derived offspring is unlikely to have substantial implications for the mutation load in laboratory populations maintained via recurrent cycles of IVF-based rederivation (Yamauchi et al. 2022) or husbandry programs that utilize ART to rederive strains at regular intervals to curtail genetic drift (Taft et al. 2006). Assuming that ~0.5% of new single nucleotide mutations are strongly deleterious (Dukler et al. 2022), a baseline mouse mutation rate of $\mu = 0.5 \times 10^{-9}$/bp/gen (Lindsay et al. 2019; Uchimura et al. 2015; López-Cortegano et al. 2025), and genome size of 2.7 Gb, we expect ~0.067 new deleterious mutations per mouse per generation under a traditional breeding program ($0.5 \times 10^{-9} \times 2.7\ \text{Gb} \times 0.005 = 0.067$). Using ART, the number of expected new deleterious mutations is increased to ~0.088 per genome per generation. Thus, for every ~50 ART-derived mice, one additional highly deleterious dnSNV is expected to be recovered compared to the natural-born

baseline. The magnitude of this impact is roughly equivalent to an increase in mouse paternal age of ~30 weeks (Lindsay et al. 2019).

While our findings reveal a moderate mutagenic impact of ART in mice, we emphasize that our conclusions cannot be readily extrapolated beyond the mouse model system profiled here. Notably, mice and humans differ in their reproductive physiology, dynamics of epigenetic reprogramming, and timeline of early embryonic development, considerations that may influence both the rate and spectrum of dnSNVs and the sensitivity of mutation accumulation under ART. Additionally, ART protocols employed in human fertility clinics typically include fertilization via ICSI, prolonged embryo culture to the blastocyst stage, and an embryo freeze-thaw cycle. These steps present clear departures from the use of naturally fertilized embryos that were freshly transferred at the 2-cell stage in our mouse protocol. Whether or how these protocol differences impact potential mutation rate differences associated with ART is unknown. In particular, prior work suggests that ICSI is associated with increased risks of birth defects compared to traditional IVF (Davies et al. 2012), lending strong motivation to future studies exploring the impact of ICSI on genome integrity. We also acknowledge that our study is limited to evaluating the effect of ART on mutation accumulation in a single genetic background (C57BL/6J). Additional studies are needed to evaluate whether our findings are generalizable across mouse strains, including mouse models of reduced fertility or infertility. Finally, while our reliance on inbred mice from a single strain background controls for inter-individual variation in mutation rate to the maximum possible extent, we cannot discount the possibility that stochastic, inter-individual differences in mutation rate contribute to the observed difference between cohorts.

While we caution that our work has no immediate implications for human clinical practice, our findings nonetheless strongly motivate further investigations to assess the potential mutagenic impact of ART in humans. This need is particularly urgent given forecasted trends toward

341 greater reliance on ART driven by sociodemographic shifts and increasing democratization of
342 access to ART (CDC 2024a).

MATERIALS AND METHODS

Animal husbandry and establishment of breeding cohorts

A single C57BL/6J breeding pair was obtained from The Jackson Laboratory and housed in a low-barrier room. All procedures were conducted in accordance with an animal care protocol approved by The Jackson Laboratory's Animal Care and Use Committee (Protocol #17021). Two G1 females from the initial litter born to this G0 C57BL/6J founder breeding pair were mated to a single male G1 littermate. One of these G1 females produced a litter of nine live-born pups and the second gave birth to a litter of seven mice (**Figure 1A**). All 16 natural-born G2 pups were reared to four weeks of age and euthanized by exposure to CO_2 prior to terminal tissue collection.

Two additional females and one male from the same G1 litter were transferred to The Jackson Laboratory's Reproductive Services Facility at four weeks of age. Females were injected with 5 IU PMSG followed 48 hours later by a 5 IU hCG trigger to induce ovulation. Oocyte clutches were then harvested from the ampullae of each superovulated female and incubated in 150µL Cook RVF media supplemented with an additional 50µL of reduced glutathione (GSH) media at 37°C under mixed gas (5% CO_2, 5% O_2, and 90% N_2) for 30-60 minutes. Concurrently, sperm were isolated from the caudal epididymides of the donor male and incubated in TYH media supplemented with 0.75mM Methyl-β-cyclodextrin at 37°C under mixed gas for 40-60 minutes.

Following incubation, egg clutches and 10µL of sperm were transferred to a 1mL drop of Cook RVF media covered with mineral oil. Fertilization occurred over approximately 2-6 hours at 37°C under mixed gas. Zygotes were then washed by transfer through two sequential droplets of Cook RVF media and incubated overnight in a final droplet of Cook RVF media at 37°C under mixed gas. Sixteen two-cell embryos from each donor female were subsequently transferred to

the oviducts of two pseudo-pregnant C57BL/6J dams and reared to term. A total of 29 live-born ART-derived G1 pups were euthanized by CO_2 at approximately four weeks of age for terminal tissue harvests (transfer to live-birth success rate: 90.6%). Of these, 12 mice (six from each litter; **Figure 1A**) were randomly selected for whole-genome sequencing (see below). Only live cells or embryos were advanced at any step of the ART protocol; no additional selection was performed on the basis of morphology or other criteria.

DNA extraction, library preparation, and sequencing

The G0 founder breeding pair, 6 G1 parents, 16 natural-born G2 mice, and 12 ART-derived G2 mice were selected for whole-genome sequencing (n = 36 samples; **Figure 1A**). Genomic DNA isolation, library preparation, and sequencing were performed in duplicate for all samples, with an initial round of data collection performed in 2020 and a second batch completed in 2023. Genomic DNA was isolated from flash-frozen mouse tails using the NucleoMag Tissue Kit (Macherey-Nagel) according to the manufacturer's protocol. Mouse tail tip tissue is composed of a mix of epidermis, dermis, peripheral nerves, blood vessels, bone, and cartilage. These tissue types include representatives from both the ectoderm (epidermis, dermis, peripheral nerves) and mesoderm cellular developmental lineages (blood vessels, bone, cartilage). DNA concentration and quality were assessed using the NanoDrop 8000 spectrophotometer (Thermo Scientific), the Qubit Flex dsDNA BR Assay (Thermo Scientific), and the Genomic DNA ScreenTape Analysis Assay (Agilent Technologies) and judged to be sufficient for library preparation for all samples. Paired-end 150 bp whole-genome libraries were constructed using the KAPA HyperPrep Kit (Roche Sequencing and Life Science) according to the manufacturer's protocols, targeting an insert size of 400 base pairs. Briefly, the protocol entails shearing the DNA using the E220 Focused-ultrasonicator (Covaris), size selection targeting 400 bp, ligation of Illumina-specific barcoded adapters and 9 bp UMI adapters, and 1 cycle of PCR amplification.

Library quality was assessed using the D5000 ScreenTape (Agilent Technologies) and concentration was determined by a Qubit dsDNA HS Assay (ThermoFisher).

The initial set of paired-end 150 bp Illumina libraries were prepared and sequenced to ~20-30× coverage on an Illumina NovaSeq 6000 using a combination of S2 and S4 flow cells. A second set of paired-end 150 bp libraries were pooled and sequenced to ~30× coverage (~90 Gb/sample) on an Illumina NovaSeq 6000 using the S4 Reagent Kit v1.5. For clarity, sequencing data from these two libraries are referred to as “Seq1” and “Seq2”.

Read processing and mapping

Read quality assessment and adaptor trimming were performed on each sample library using fastp (v. 0.23.4) (Chen 2023). Processed reads were then mapped to the GRCm39 mouse reference genome using default parameters in BWA MEM (v. 0.7.17-r1188) (Li and Durbin 2009) and indexed using SAMtools (v. 1.21) (Li et al. 2009). Duplicate reads were identified using a series of SAMtools commands:

```
samtools collate -O -u $BAM_FILE | \
    samtools fixmate -m -u - - | \
    samtools sort -u - | \
    samtools markdup --use-read-groups -f $STATS_FILE \
        -S -d 2500 --mode s --include-fails - $MARKED_BAM_FILE
```

Mapping metrics were computed for each sequenced library using the flagstat and idxstats commands in SAMtools (**Supplemental Table 1**). The two independent libraries generated from each sample were then merged using SAMtools, and mapping metrics re-computed on the merged file (**Supplemental Table 1**).

Single nucleotide variant calling

Single sample variant calling was performed using DeepVariant (v. 1.6.1) with the pre-trained WGS model (Poplin et al. 2018; Yun et al. 2021). A joint call set including all 36 samples was derived using GLnexus (v. 1.2.7) (Yun et al. 2021). In parallel, we used mpileup was run via the 'bcftools call' command in BCFtools (v. 1.9-1) with default parameters to produce a second joint call set (Li 2011). These variant calling steps were executed on the individual Seq1 and Seq2 BAM files from each sample, as well as the merged BAM file integrating data from both Seq1 and Seq2. Calls from the merged data were used as the primary source for dnSNV discovery (see below), with the Seq1 and Seq2 call sets offering supportive confirmation of dnSNVs in two independent libraries.

De novo mutation discovery

dnSNV discovery was performed using the joint SNV call sets generated from merged BAM files containing reads from both sequencing libraries (Seq1 and Seq2). The joint VCF file was filtered using BCFtools (v. 1.16) (Danecek et al. 2021) to retain only autosomal, biallelic SNVs that were present in a heterozygous state in a single G2 individual and absent from all other individuals in the pedigree. Following simulation-based recommendations for dnSNV discovery in mice, we retained only calls supported by both mpileup and DeepVariant and applied regional filters to remove dnSNVs residing in genomic regions prone to false-positives (Garretson et al. 2025). Specifically, putative dnSNVs were excluded if they (i) overlapped with any of the following annotations defined by the RepeatMasker track accessed from the UCSC Genome Browser (Kent et al. 2002): low complexity regions, rRNA, satellite DNA, scRNA, simple repeats, snRNA, srpRNA, and tRNA; (ii) were flanked on one or both sides by an A/T homopolymer run >5 bp; (iii) were located within 35 bp of another SNV; or (iv) overlapped a manually-curated set of highly copy number variable genes in the mouse genome (**Supplemental Table 6**). We next ensured that putative G2 dnSNVs surviving these strict filters were independently supported by calls in both Seq1 and Seq2. This step eliminated <5% of identified dnSNVs, revealing high

concordance between the two sequenced libraries. The final set of dnSNVs is provided in **Supplemental Table 2**.

We employed an identical procedure for dnSNV discovery in the individual Seq1 and Seq2 data sets, excluding the requirement that dnSNVs are confirmed by both sequence batches (**Supplemental Tables 3 and 4**).

De novo mutation rate estimation and analysis of mutation spectrum

To assess differences in de novo mutation counts between cohorts, we fit a generalized linear model with the form Count ~ Cohort using the MASS package in R (Venables and Ripley 2002). dnSNV counts were modeled as a negative binomial random variable with a log link function, rather than a Poisson random variable, as preliminary exploration of the count data revealed mild overdispersion (mean = 19.4, variance = 35.1). Nonetheless, our findings are robust to distributional assumptions (Poisson: IRR = 1.276, 95% CI: 1.078 - 1.510, P = 0.0046; Negative Binomial: IRR = 1.276 (95% CI: 1.045 - 1.558), P = 0.017). The cohort effect was interpreted on the multiplicative scale as an incident rate ratio (IRR), specifying the natural mating cohort as the reference.

The per base de novo mutation rate (μ) was estimated for each G2 sample using the following formula:

$$\mu = \frac{M}{(2 \times G)},$$

where M is the number of dnSNVs per G2 sample, and G is the effective haploid genome size in base pairs. G was calculated as the total length of the 19 mouse autosomes (2.44 Gb) minus masked regions described above, resulting in an effective genome size of 2.23 Gb.

De novo SNV spectra were obtained for each G2 sample using the TsTv-summary output flag in VCFtools (v. 0.1.16) (Danecek et al. 2011). dnSNVs were further annotated by their trinucleotide

context (i.e., the focal dnSNV and its immediate 3' and 5' flanking nucleotides) using the R libraries SomaticSignatures (v. 2.38.2) (Gehring et al. 2015) and VariantAnnotation (v. 1.48.1) (Obenchain et al. 2014). We used a modified Chi-square test with *P*-values corrected for non-independence to test for differences in the fraction of each mutational type between the two cohorts, following the approach described by Harris and Prichard (2017). We then aggregated the trinucleotide spectra across our two breeding cohorts to assess relationships with defined COSMIC single-base mutation signatures (v. 3.4) (Alexandrov et al. 2020) for the mouse reference genome (mm10) using SigProfilerAssignment in Python (v. 0.2.3) (Díaz-Gay et al. 2023). Because both ART-derived and natural-born cohorts feature individuals not exposed to environmental toxins or chemotherapeutics, we excluded mutation signatures not relevant to our unexposed samples (e.g., aristolochic acid, colibactin, UV damage, tobacco smoking, and chemotherapy treatment signatures), applying this filter to all samples.

To evaluate the statistical significance of signature contributions between the two cohorts, we randomly shuffled the cohort labels of dnSNVs in their trinucleotide contexts and re-computed mutation signatures. We then compared the observed absolute cohort difference in trinucleotide mutation proportions to a null distribution of 1000 randomly permuted differences. A *P*-value was calculated as the probability of observing a difference as large or larger than the observed difference. All statistical analyses were performed in R (v. 4.2.2) and RStudio (v. 4.2.2) (R Core Team 2023).

Genomic annotation and epigenomic enrichment of dnSNVs

dnSNVs were annotated using SnpEff (v. 5.0) (Cingolani et al. 2012). The intersect command within BEDTools (v. 2.28.0) (Quinlan and Hall 2010) was used to determine the numbers of dnSNVs overlapping various classes of repeat elements annotated in the GRCm39/mm39 reference genome using the RepeatMasker track extracted from UCSC Table Browser (Kent et al. 2002). Similarly, we interrogated SNP locations over CpG islands by intersecting dnSNVs

with the 'CpG Island' track from the UCSC Genome Browser. To compare GC content between cohorts, we calculated GC content within a 201 bp window centered on each dnSNV and contrasted the resulting cohort-specific distributions.

BEDTools was used to intersect dnSNVs with CTCF binding sites and various histone modifications assayed by ChIP-seq in C57BL/6J mouse ESCs under the Mouse ENCODE Project (Stamatoyannopoulos et al. 2012) and early mouse embryos (Liu et al. 2016). dnSNV coordinates were first lifted over to mm10 reference genome coordinates to ensure compatibility with ChIP-seq peak positions reported in ENCODE datasets. Differential enrichment of dnSNVs between cohorts was assessed by Fisher's exact tests. Similarly, dnSNVs were intersected with quantitative estimates of transcript abundance in C57BL/6J mouse ESCs (Stamatoyannopoulos et al. 2012), specifying a 2.5 kb window upstream of the gene start and downstream of the gene end. Cohort differences in the mean expression level of genes neighboring dnSNVs and the proportion of dnSNVs neighboring active versus inactive genes were assessed by a two-tailed Wilcoxon rank-sum test and a Fisher's exact test, respectively. To evaluate potential cohort differences in the replication timing of genomic regions where dnSNVs arise, dnSNVs were intersected with published Repli-seq replication timing estimates on mESCs (Pratto et al. 2021; Dey et al. 2015). Shifts in the distribution of replication timepoints between ART-derived and natural-born mice were evaluated by two-tailed Wilcoxon rank-sum tests.

Structural variant calling and de novo structural variant discovery

SV discovery was performed on each cohort using DELLY (v. 0.8.7) (Rausch et al. 2012) and Manta (v. 1.6.0) (Chen et al. 2016). We used default settings in DELLY to perform per sample germline SV calling against the GRCm39 reference and subsequently merged calls across all samples in our pedigree. In parallel, we used Manta to jointly call germline SVs in each of the 28 parent-offspring trios embedded in our pedigree (**Figure 1A**), followed by merging of these per trio SV call sets. (Running a joint sample analysis with Manta on larger sample sets caused run

time challenges and proved to be infeasible with our compute resources). We then intersected the two final SV call sets from Manta and DELLY using the *collapse* command in Truvari (v. 4.0.0) (English et al. 2022) with the following parameters: -pctsize 0.75 –pctovl 0.5 –pctseq 0.7 -s 20 -S 10000000 -k common --chain. We retained only calls that were supported by both callers and that were unique to a single G2 sample. We focused on deletions and duplications, excluding complex and copy number neutral SVs due to the inherent limitations of short-read data. These candidate de novo SVs were then visually inspected for read depth signatures consistent with duplications and deletion calls using Samplot (v. 1.1.6) (Belyeu et al. 2021b). Only calls visually supported by expected read depth patterns were retained. This manual filter resulted in the exclusion of 462 deletions and 108 duplications. De novo SVs were annotated for predicted functional effects using the Ensembl variation effect predictor (v. 2.0) (McLaren et al. 2016). Cohort-level differences in de novo SV rate were evaluated by fitting a negative binomial regression, as for dnSNVs.

DATA ACCESS

All sequencing data from this study have been submitted to the NCBI BioProject database (https://www.ncbi.nlm.nih.gov/bioproject/) under accession number PRJNA1282662. Code required to reproduce our analysis is available on Figshare (https://doi.org/10.6084/m9.figshare.30179809.v1).

COMPETING INTEREST STATEMENT

The authors have no competing interests to disclose.

ACKNOWLEDGEMENTS

We thank members of the Dumont Lab, Baker Lab, and Mary Ann Handel at The Jackson Laboratory for critical feedback on this project. We are indebted to the technical expertise of the scientific staff in The Jackson Laboratory's Reproductive Sciences and Genome Technologies Scientific Service for carrying out ART procedures and whole-genome sequencing, respectively. We also thank the Research IT Staff at The Jackson Laboratory for their oversight and maintenance of the high-performance computing resources that made this work possible. This work was supported by start-up funds from The Jackson Laboratory and a MIRA from The National Institute of General Medical Sciences to BLD (R35 GM133415).

Author Contributions: BLD and LBB conceptualized and designed the project. LBB performed all experimental investigation and led formal analysis, with supervision and funding support from BLD. BLD and AG contributed to formal analysis and data visualization. LBB and BLD wrote the original manuscript draft, with substantial input and review from AG.

REFERENCES

Alexandrov LB, Kim J, Haradhvala NJ, Huang MN, Tian Ng AW, Wu Y, Boot A, Covington KR, Gordenin DA, Bergstrom EN, et al. 2020. The repertoire of mutational signatures in human cancer. *Nature* **578**: 94–101.

Barberet J, Binquet C, Guilleman M, Doukani A, Choux C, Bruno C, Bourredjem A, Chapusot C, Bourc'his D, Duffourd Y, et al. 2021. Do assisted reproductive technologies and *in vitro* embryo culture influence the epigenetic control of imprinted genes and transposable elements in children? *Hum Reprod* **36**: 479–492.

Bean CJ. 2002. Fertilization in vitro increases non-disjunction during early cleavage divisions in a mouse model system. *Hum Reprod* **17**: 2362–2367.

Belyeu JR, Brand H, Wang H, Zhao X, Pedersen BS, Feusier J, Gupta M, Nicholas TJ, Brown J, Baird L, et al. 2021a. De novo structural mutation rates and gamete-of-origin biases revealed through genome sequencing of 2,396 families. *Am J Hum Genet* **108**: 597–607.

Belyeu JR, Chowdhury M, Brown J, Pedersen BS, Cormier MJ, Quinlan AR, Layer RM. 2021b. Samplot: a platform for structural variant visual validation and automated filtering. *Genome Biol* **22**: 161.

Bergeron LA, Besenbacher S, Zheng J, Li P, Bertelsen MF, Quintard B, Hoffman JI, Li Z, St. Leger J, Shao C, et al. 2023. Evolution of the germline mutation rate across vertebrates. *Nature* **615**: 285–291.

Bonduelle M. 2002. Prenatal testing in ICSI pregnancies: incidence of chromosomal anomalies in 1586 karyotypes and relation to sperm parameters. *Hum Reprod* **17**: 2600–2614.

Bristow RG, Hill RP. 2008. Hypoxia, DNA repair and genetic instability. *Nat Rev Cancer* **8**: 180–192.

Bruno M, Maisha S, Mitra A, Costello K, Watkins-Chow D, Logsdon GA, Gambogi CW, Dumont BL, Black BE, Keane TM, et al. 2025. Young KRAB-zinc finger gene clusters are highly dynamic incubators of ERV-driven genetic heterogeneity in mice. bioRxiv doi: 10.1101/2025.02.26.640358.

Caperton L, Murphey P, Yamazaki Y, McMahan CA, Walter CA, Yanagimachi R, McCarrey JR. 2007. Assisted reproductive technologies do not alter mutation frequency or spectrum. *Proc Natl Acad Sci USA* **104**: 5085–5090.

CDC. 2024a. National ART Summary. *Assisted Reproductive Technology (ART)*. https://www.cdc.gov/art/php/national-summary/index.html (Accessed June 20, 2025).

CDC. 2024b. State-Specific ART Surveillance. *Assisted Reproductive Technology (ART)*. https://www.cdc.gov/art/php/surveillance-state-specific/index.html (Accessed June 20, 2025).

Chen C, Qi H, Shen Y, Pickrell J, Przeworski M. 2017. Contrasting Determinants of Mutation Rates in Germline and Soma. *Genetics* **207**: 255–267.

Chen S. 2023. Ultrafast one-pass FASTQ data preprocessing, quality control, and deduplication using fastp. *iMeta* **2**: e107.

Chen X, Schulz-Trieglaff O, Shaw R, Barnes B, Schlesinger F, Källberg M, Cox AJ, Kruglyak S, Saunders CT. 2016. Manta: rapid detection of structural variants and indels for germline and cancer sequencing applications. *Bioinformatics* **32**: 1220–1222.

Choux C, Binquet C, Carmignac V, Bruno C, Chapusot C, Barberet J, Lamotte M, Sagot P, Bourc'his D, Fauque P. 2018. The epigenetic control of transposable elements and imprinted genes in newborns is affected by the mode of conception: ART versus spontaneous conception without underlying infertility. *Hum Reprod* **33**: 331–340.

Cingolani P, Platts A, Wang LL, Coon M, Nguyen T, Wang L, Land SJ, Lu X, Ruden DM. 2012. A program for annotating and predicting the effects of single nucleotide polymorphisms, SnpEff: SNPs in the genome of Drosophila melanogaster strain w1118; iso-2; iso-3. *Fly (Austin)* **6**: 80–92.

Cortessis VK, Azadian M, Buxbaum J, Sanogo F, Song AY, Sriprasert I, Wei PC, Yu J, Chung K, Siegmund KD. 2018. Comprehensive meta-analysis reveals association between multiple imprinting disorders and conception by assisted reproductive technology. *J Assist Reprod Genet* **35**: 943.

Currie CE, Ford E, Benham Whyte L, Taylor DM, Mihalas BP, Erent M, Marston AL, Hartshorne GM, McAinsh AD. 2022. The first mitotic division of human embryos is highly error prone. *Nat Commun* **13**: 6755.

Danecek P, Auton A, Abecasis G, Albers CA, Banks E, DePristo MA, Handsaker RE, Lunter G, Marth GT, Sherry ST, et al. 2011. The variant call format and VCFtools. *Bioinformatics* **27**: 2156–2158.

Danecek P, Bonfield JK, Liddle J, Marshall J, Ohan V, Pollard MO, Whitwham A, Keane T, McCarthy SA, Davies RM, Li H. 2021. Twelve years of SAMtools and BCFtools. *Gigascience* **10**: giab008.

Daugelaite K, Lacour P, Winkler I, Koch M-L, Schneider A, Schneider N, Tolkachov A, Nguyen XP, Vilkaite A, Rehnitz J, et al. 2023. Superovulation and aging perturb oocyte-granulosa cell communication. bioRxiv doi: 10.1101/2023.10.30.563978.

Davies MJ, Moore VM, Willson KJ, Essen PV, Priest K, Scott H, Haan EA, Chan A. 2012. Reproductive Technologies and the Risk of Birth Defects. *N Engl J Med* **366**: 1803–1813.

de Waal E, Vrooman LA, Fischer E, Ord T, Mainigi MA, Coutifaris C, Schultz RM, Bartolomei MS. 2015. The cumulative effect of assisted reproduction procedures on placental development and epigenetic perturbations in a mouse model. *Hum Mol Genet* **24**: 6975–6985.

Dey SS, Kester L, Spanjaard B, Bienko M, van Oudenaarden A. 2015. Integrated genome and transcriptome sequencing of the same cell. *Nat Biotechnol* **33**: 285–289.

Díaz-Gay M, Vangara R, Barnes M, Wang X, Islam SMA, Vermes I, Duke S, Narasimman NB, Yang T, Jiang Z, et al. 2023. Assigning mutational signatures to individual samples and individual somatic mutations with SigProfilerAssignment. *Bioinformatics* **39**: btad756.

Dukler N, Mughal MR, Ramani R, Huang Y-F, Siepel A. 2022. Extreme purifying selection against point mutations in the human genome. *Nat Commun* **13**: 4312.

English AC, Menon VK, Gibbs RA, Metcalf GA, Sedlazeck FJ. 2022. Truvari: refined structural variant comparison preserves allelic diversity. *Genome Biol* **23**: 271.

ESHRE Factsheet on ART. 2005. https://www.eshre.eu/Press-Room/Resources/Fact-sheets (Accessed July 10, 2025).

Garcia-Salinas OI, Hwang S, Huang QQ, Sanghvi R, Malawsky DS, Kaplanis J, Neville MDC, Day FR, Rahbari R, Scally A, et al. 2025. The impact of ancestral, genetic, and environmental influences on germline de novo mutation rates and spectra. *Nat Commun* **16**: 4527.

Garretson A, Blanco-Berdugo L, Roberts A, Dumont BL. 2025. Benchmarking Genomic Variant Calling Tools in Inbred Mouse Strains: Recommendations and Considerations. bioRxiv doi: 10.1101/2025.05.28.656711.

Gehring JS, Fischer B, Lawrence M, Huber W. 2015. SomaticSignatures: inferring mutational signatures from single-nucleotide variants, *Bioinformatics* 31: 3673–3675.

Ghosh J, Coutifaris C, Sapienza C, Mainigi M. 2017. Global DNA methylation levels are altered by modifiable clinical manipulations in assisted reproductive technologies. *Clin Epigenetics* **9**: 14.

Gille JJ, van Berkel CG, Joenje H. 1994. Mutagenicity of metabolic oxygen radicals in mammalian cell cultures. *Carcinogenesis* **15**: 2695–2699.

Giritharan G, Talbi S, Donjacour A, Di Sebastiano F, Dobson AT, Rinaudo PF. 2007. Effect of in vitro fertilization on gene expression and development of mouse preimplantation embryos. *Reproduction* **134**: 63–72.

Håberg SE, Page CM, Lee Y, Nustad HE, Magnus MC, Haftorn KL, Carlsen EØ, Denault WRP, Bohlin J, Jugessur A, et al. 2022. DNA methylation in newborns conceived by assisted reproductive technology. *Nat Commun* **13**: 1896.

Hansen M, Kurinczuk JJ, Milne E, de Klerk N, Bower C. 2013. Assisted reproductive technology and birth defects: a systematic review and meta-analysis. *Hum Reprod Update* **19**: 330–353.

Harris K, Pritchard JK. 2017. Rapid evolution of the human mutation spectrum. *eLife* **6**: e24284.

Hart RJ, Wijs LA. 2022. The longer-term effects of IVF on offspring from childhood to adolescence. *Front Reprod Health* **4**: 1045762.

Hassold T, Hunt P. 2001. To err (meiotically) is human: the genesis of human aneuploidy. *Nat Rev Genet* **2**: 280–291.

Hattori H, Hiura H, Kitamura A, Miyauchi N, Kobayashi N, Takahashi S, Okae H, Kyono K, Kagami M, Ogata T, et al. 2019. Association of four imprinting disorders and ART. *Clin Epigenetics* **11**: 21.

Hayashi S. 2003. Mouse Preimplantation Embryos Developed from Oocytes Injected with Round Spermatids or Spermatozoa Have Similar but Distinct Patterns of Early Messenger RNA Expression. *Biol Reprod* **69**: 1170–1176.

Katagiri Y, Jwa SC, Kuwahara A, Iwasa T, On M, Kato K, Kishi H, Kuwabara Y, Taniguchi F, Harada M, et al. 2023. Assisted reproductive technology in Japan: A summary report for 2021 by the Ethics Committee of the Japan Society of Obstetrics and Gynecology. *Reprod Med Biol* **23**: e12552.

Kent WJ, Sugnet CW, Furey TS, Roskin KM, Pringle TH, Zahler AM, Haussler and D. 2002. The Human Genome Browser at UCSC. *Genome Res* **12**: 996–1006.

Kohda T. 2013. Effects of embryonic manipulation and epigenetics. *J Hum Genet* **58**: 416–420.

Konstantogianni O, Panou T, Zikopoulos A, Skentou C, Stavros S, Asimakopoulos B. 2024. Culture of Human Embryos at High and Low Oxygen Levels. *J Clin Med* **13**: 2222.

Koustas G, Sjoblom C. 2016. Minute changes to the culture environment of mouse pre-implantation embryos affect the health of the conceptus. *Asian Pac J Reprod* **5**: 287–294.

Lee Y-L, Bouwman AC, Harland C, Bosse M, Moreira GCM, Veerkamp RF, Mullaart E, Cambisano N, Groenen MAM, Karim L, et al. 2023. The rate of de novo structural variation is increased in in vitro–produced offspring and preferentially affects the paternal genome. *Genome Res* **33**: 1455–1464.

Li H. 2011. A statistical framework for SNP calling, mutation discovery, association mapping and population genetical parameter estimation from sequencing data. *Bioinformatics* **27**: 2987–2993.

Li H, Durbin R. 2009. Fast and accurate short read alignment with Burrows–Wheeler transform. *Bioinformatics* **25**: 1754–1760.

Li H, Handsaker B, Wysoker A, Fennell T, Ruan J, Homer N, Marth G, Abecasis G, Durbin R. 2009. The Sequence Alignment/Map format and SAMtools. *Bioinformatics* **25**: 2078–2079.

Lindsay SJ, Rahbari R, Kaplanis J, Keane T, Hurles ME. 2019. Similarities and differences in patterns of germline mutation between mice and humans. *Nat Commun* **10**: 4053.

Liu X, Wang C, Liu W, Li J, Li C, Kou X, Chen J, Zhao Y, Gao H, Wang H, et al. 2016. Distinct features of H3K4me3 and H3K27me3 chromatin domains in pre-implantation embryos. *Nature* **537**: 558–562.

Lopes JS, Ivanova E, Ruiz S, Andrews S, Kelsey G, Coy P. 2022. Effect of Superovulation Treatment on Oocyte's DNA Methylation. *Int J Mol Sci* **23**: 16158.

López-Cortegano E, Chebib J, Jonas A, Vock A, Künzel S, Keightley PD, Tautz D. 2025. The rate and spectrum of new mutations in mice inferred by long-read sequencing. *Genome Res* **35**: 43–54.

López-Cortegano E, Chebib J, Jonas A, Vock A, Künzel S, Tautz D, Keightley PD. 2024. Variation in the Spectrum of New Mutations among Inbred Strains of Mice. *Mol Biol Evol* **41**: msae163.

Luke B, Brown MB, Wantman E, Forestieri NE, Browne ML, Fisher SC, Yazdy MM, Ethen MK, Canfield MA, Watkins S, et al. 2021. The risk of birth defects with conception by ART. *Hum Reprod* **36**: 116–129.

Makova KD, Hardison RC. 2015. The effects of chromatin organization on variation in mutation rates in the genome. *Nat Rev Genet* **16**: 213–223.

Mani S, Ghosh J, Coutifaris C, Sapienza C, Mainigi M. 2019. Epigenetic changes and assisted reproductive technologies. *Epigenetics* **15**: 12.

Market-Velker BA, Zhang L, Magri LS, Bonvissuto AC, Mann MRW. 2010. Dual effects of superovulation: loss of maternal and paternal imprinted methylation in a dose-dependent manner. *Hum Mol Genet* **19**: 36–51.

McDonald SD, Han Z, Mulla S, Murphy KE, Beyene J, Ohlsson A, Knowledge Synthesis Group. 2009. Preterm birth and low birth weight among in vitro fertilization singletons: a systematic review and meta-analyses. *Eur J Obstet Gynecol Reprod Biol* **146**: 138–148.

McLaren W, Gil L, Hunt SE, Riat HS, Ritchie GRS, Thormann A, Flicek P, Cunningham F. 2016. The Ensembl Variant Effect Predictor. *Genome Biol* **17**: 122.

Moore L, Cagan A, Coorens THH, Neville MDC, Sanghvi R, Sanders MA, Oliver TRW, Leongamornlert D, Ellis P, Noorani A, et al. 2021. The mutational landscape of human somatic and germline cells. *Nature* **597**: 381–386.

Nugent CN, Chandra A. 2024. *Infertility and Impaired Fecundity in Women and Men in the United States, 2015–2019*. National Center for Health Statistics (U.S.), Hyattsville, MD https://stacks.cdc.gov/view/cdc/147886 (Accessed October 18, 2024).

Obenchain V, Lawrence M, Carey V, Gogarten S, Shannon P, Morgan M. 2014. VariantAnnotation: a Bioconductor package for exploration and annotation of genetic variants. *Bioinformatics* 30: 2076–2078.

Ooga M, Kikuchi Y, Ito D, Kazama K, Inoue R, Sakamoto M, Wakayama S, Wakayama T. 2023. Aberrant histone methylation in mouse early preimplantation embryos derived from round spermatid injection. *Biochem Biophys Res Commun* **680**: 119–126.

Osterman MJ, Hamilton BE, Martin JA, Driscoll AK, Valenzuela CP. 2025. Births: Final Data for 2023. *National Vital Statistics Reports* **74**.

Palomba S, Homburg R, Santagni S, La Sala GB, Orvieto R. 2016. Risk of adverse pregnancy and perinatal outcomes after high technology infertility treatment: a comprehensive systematic review. *Reprod Biol Endocrinol* **14**: 76.

728 Pleasance ED, Cheetham RK, Stephens PJ, McBride DJ, Humphray SJ, Greenman CD, Varela
729 I, Lin M-L, Ordóñez GR, Bignell GR, et al. 2010. A comprehensive catalogue of somatic
730 mutations from a human cancer genome. *Nature* **463**: 191–196.

731 Poplin R, Chang PC, Alexander D, Schwartz S, Colthurst T, Ku A, Newburger D, Dijamco J,
732 Nguyen N, Afshar PT, et al. 2018. A universal SNP and small-indel variant caller using
733 deep neural networks. *Nat Biotechnol*. 36: 983-987.

734 Pratto F, Brick K, Cheng G, Lam K-WG, Cloutier JM, Dahiya D, Wellard SR, Jordan PW,
735 Camerini-Otero RD. 2021. Meiotic recombination mirrors patterns of germline replication in
736 mice and humans. *Cell* **184**: 4251-4267.e20.

737 Quinlan AR, Hall IM. 2010. BEDTools: a flexible suite of utilities for comparing genomic
738 features, *Bioinformatics*. 26: 841–842.

739 R Core Team. 2023. R: A Language and Environment for Statistical Computing. R Foundation
740 for Statistical Computing, Vienna, Austria. <https://www.R-project.org/>.

741 Rausch T, Zichner T, Schlattl A, Stütz AM, Benes V, Korbel JO. 2012. DELLY: structural variant
742 discovery by integrated paired-end and split-read analysis. *Bioinformatics* **28**: i333–i339.

743 Reik W, Dean W, Walter J. 2001. Epigenetic reprogramming in mammalian development.
744 *Science* **293**: 1089–1093.

745 Rivera RM, Stein P, Weaver JR, Mager J, Schultz RM, Bartolomei MS. 2008. Manipulations of
746 mouse embryos prior to implantation result in aberrant expression of imprinted genes on
747 day 9.5 of development. *Hum Mol Genet* **17**: 1–14.

748 Ruth KS, Day FR, Hussain J, Martínez-Marchal A, Aiken CE, Azad A, Thompson DJ,
749 Knoblochova L, Abe H, Tarry-Adkins JL, et al. 2021. Genetic insights into biological
750 mechanisms governing human ovarian ageing. *Nature* **596**: 393–397.

751 Smeenk J, Wyns C, De Geyter C, Kupka M, Bergh C, Cuevas Saiz I, De Neubourg D, Rezabek
752 K, Tandler-Schneider A, Rugescu I, et al. 2023. ART in Europe, 2019: results generated
753 from European registries by ESHRE. *Hum Reprod* **38**: 2321–2338.

754 Song S, Ghosh J, Mainigi M, Turan N, Weinerman R, Truongcao M, Coutifaris C, Sapienza C.
755 2015. DNA methylation differences between in vitro- and in vivo-conceived children are
756 associated with ART procedures rather than infertility. *Clin Epigenetics* **7**: 41.

757 Stamatoyannopoulos JA, Adzhubei I, Thurman RE, Kryukov GV, Mirkin SM, Sunyaev SR. 2009.
758 Human mutation rate associated with DNA replication timing. *Nat Genet* **41**: 393–395.

759 Stamatoyannopoulos JA, Snyder M, Hardison R, Ren B, Gingeras T, Gilbert DM, Groudine M,
760 Bender M, Kaul R, Canfield T, et al. 2012. An encyclopedia of mouse DNA elements
761 (Mouse ENCODE). *Genome Biol* **13**: 418.

762 Taft RA, Davisson M, Wiles MV. 2006. Know thy mouse. *Trends Genet* **22**: 649–653.

763 Tan K, Zhang Z, Miao K, Yu Y, Sui L, Tian J, An L. 2016. Dynamic integrated analysis of DNA
764 methylation and gene expression profiles in in vivo and in vitro fertilized mouse post-
765 implantation extraembryonic and placental tissues. *Mol Hum Reprod* **22**: 485–498.

766 Uchimura A, Higuchi M, Minakuchi Y, Ohno M, Toyoda A, Fujiyama A, Miura I, Wakana S,
767 Nishino J, Yagi T. 2015. Germline mutation rates and the long-term phenotypic effects of
768 mutation accumulation in wild-type laboratory mice and mutator mice. *Genome Res* **25**:
769 1125–1134.

770 Vanneste E, Voet T, Le Caignec C, Ampe M, Konings P, Melotte C, Debrock S, Amyere M,
771 Vikkula M, Schuit F, et al. 2009. Chromosome instability is common in human cleavage-
772 stage embryos. *Nat Med* **15**: 577–583.

773 Venables WN, Ripley BD. 2002. Modern Applied Statistics with S. 4th ed. Springer, New York.

774 Wang C, Lv H, Ling X, Li H, Diao F, Dai J, Du J, Chen T, Xi Q, Zhao Y, et al. 2021. Association
775 of assisted reproductive technology, germline de novo mutations and congenital heart
776 defects in a prospective birth cohort study. Cell Res 31: 919–928.

777 Xie J-K, Wang Q, Chen Y-H, Tang S-B, Sun H-Y, Ge Z-J, Zhang CL. 2024. Effects of
778 multisuperovulation on the transcription and genomic methylation of oocytes and offspring.
779 *Clin Epigenet* **16**: 135.

780 Yamauchi Y, Matsumura T, Bakse J, Holmlund H, Blanchet G, Carrot E, Ikawa M, Ward MA.
781 2022. Loss of mouse Y chromosome gene Zfy1 and Zfy2 leads to spermatogenesis
782 impairment, sperm defects, and infertility. *Biol Reprod* **106**: 1312–1326.

783 Yu B, Smith TH, Battle SL, Ferrell S, Hawkins RD. 2019. Superovulation alters global DNA
784 methylation in early mouse embryo development. *Epigenetics* **14**: 780–790.

785 Yue F, Cheng Y, Breschi A, Vierstra J, Wu W, Ryba T, Sandstrom R, Ma Z, Davis C, Pope BD,
786 et al. 2014. A comparative encyclopedia of DNA elements in the mouse genome. *Nature*
787 **515**: 355–364.

788 Yun T, Li H, Chang P-C, Lin MF, Carroll A, McLean CY. 2021. Accurate, scalable cohort variant
789 calls using DeepVariant and GLnexus. *Bioinformatics* **36**: 5582–5589.

790 Zamani Esteki M, Viltrop T, Tšuiko O, Tiirats A, Koel M, Nõukas M, Žilina O, Teearu K,
791 Marjonen H, Kahila H, et al. 2019. In vitro fertilization does not increase the incidence of de
792 novo copy number alterations in fetal and placental lineages. *Nat Med* **25**: 1699–1705.

793 Zhang Z, Li L, Duan Y, Zhou J, Gao S, Cui L. 2025. The effect of in vitro fertilization on the
794 cardiac health of mice. *BMC Cardiovasc Disord* **25**: 480.

795 Zhao C, Biondic S, Vandal K, Björklund ÅK, Hagemann-Jensen M, Sommer TM, Canizo J, Clark
796 S, Raymond P, Zenklusen DR, et al. 2022. Single-cell multi-omics of human
797 preimplantation embryos shows susceptibility to glucocorticoids. *Genome Res* **32**: 1627–
798 1641.

799

FIGURE LEGENDS

Figure 1. dnSNV rates in ART-derived and natural-born mice. (A) A single founder mating pair (green; G0) produced six G1 breeders that were used to establish two cohorts, one derived by natural mating (purple) and the other derived through a series of ART procedures (orange). Each cohort consists of two litters of half-siblings. Circles represent females and squares represent males. (B) Boxplots showing the median, interquartile range, and full range of dnSNV rates per bp/generation across G2 samples. (C) Boxplots summarizing sample- and cohort-level variation in the relative transition and transversion rates and (D) mutational types. In panels B-D, data points derived from G2 females are depicted as circles and G2 males are represented by triangles.

Figure 2. Comparison of mutational trinucleotide context and COSMIC single-base signatures across ART-derived and natural-born G2 samples. (A) Bar plot of the relative contribution of COSMIC single-base signatures to the proportion of observed dnSNVs in the ART and natural birth cohorts. Permutation testing indicates no significant differences in signature contributions between cohorts. (B) Heatmap displaying the ratio of the average proportions of each of the 96 trinucleotide mutational contexts between ART-derived and natural-born samples. White boxes indicate that the mutational type was absent in both cohorts, and grey hashing indicates that the mutation type was only present in ART samples and absent in natural-born G2 mice, rendering ratios as undefined. The asterisk indicates a significant difference in the C[C>A]A trinucleotide mutation fraction between the two cohorts.

Figure 3. The genomic landscape of dnSNVs in natural-born and ART-derived mice. (A) Proportion of dnSNVs that reside in genomic regions assigned to various functional annotations. (B) Proportion of dnSNVs in natural and ART genomes assigned to “Modifier” and “Low” functional effect predictions. (C) The percentage of dnSNVs overlapping TE repeat classes in

824 the two breeding cohorts. We find no significant cohort-level differences in dnSNV enrichment in
825 any of these annotation categories.

Figure 1.

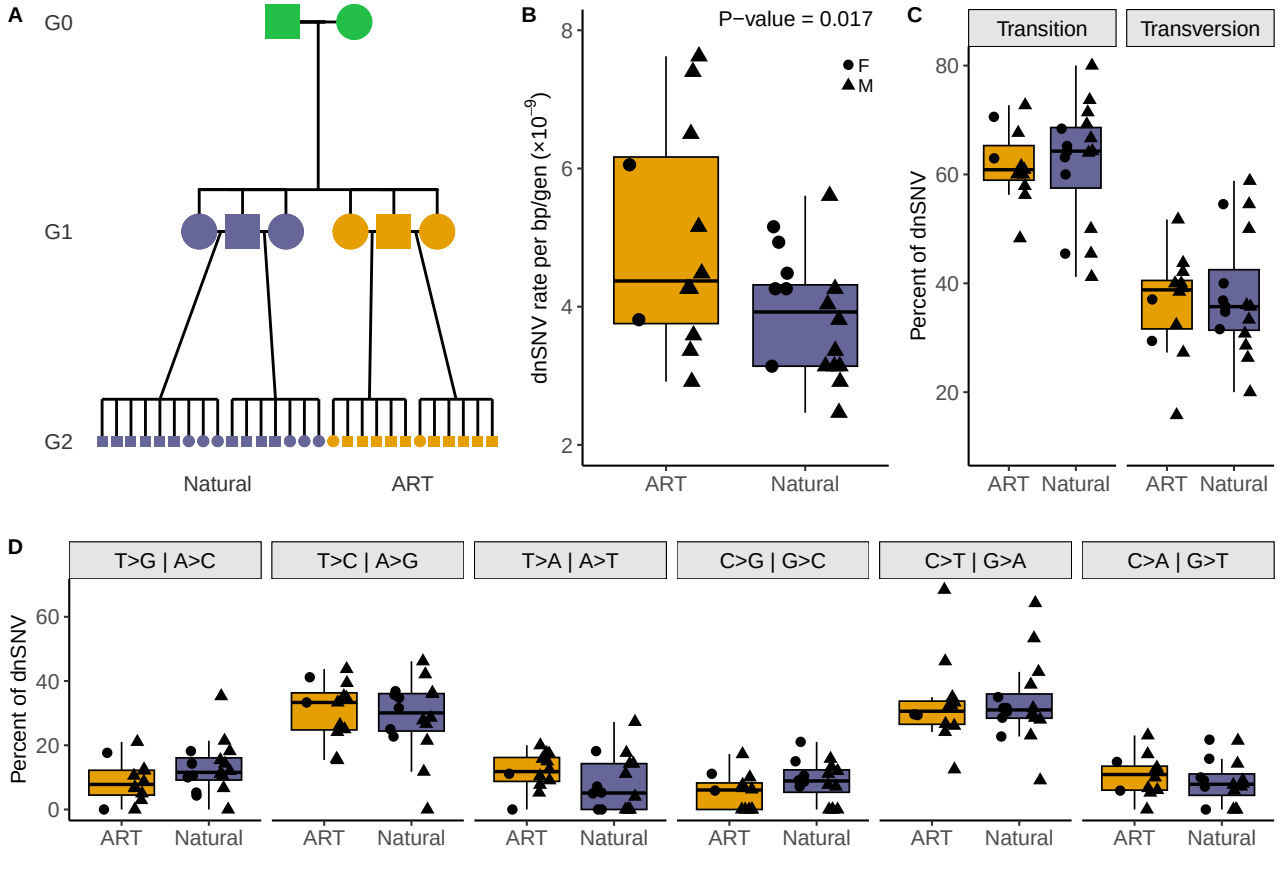
A
G0
G1
G2
Natural
ART
B
P−value = 0.017
F
M
dnSNV rate per bp/gen (×10−9)
8
6
4
2
ART
Natural
C
Transition
Transversion
Percent of dnSNV
80
60
40
20
ART
Natural
ART
Natural
D
T>G | A>C
T>C | A>G
T>A | A>T
C>G | G>C
C>T | G>A
C>A | G>T
Percent of dnSNV
60
40
20
0
ART
Natural

Figure 2.

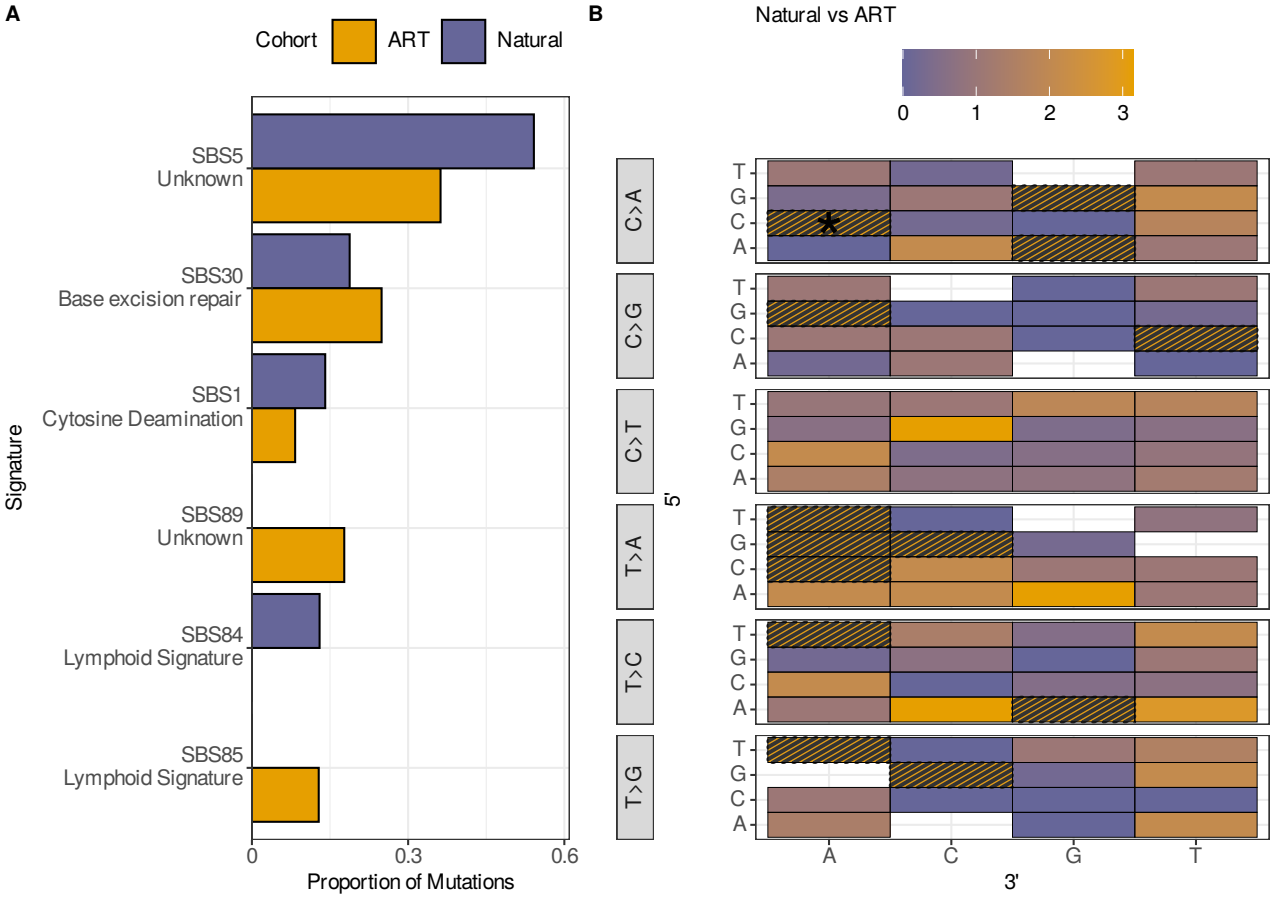
A
Cohort
ART
Natural
SBS5
Unknown
SBS30
Base excision repair
SBS1
Cytosine Deamination
SBS89
Unknown
SBS84
Lymphoid Signature
SBS85
Lymphoid Signature
Signature
0
0.3
0.6
Proportion of Mutations
B
Natural vs ART
0
1
2
3
C>A
C>G
C>T
T>A
T>C
T>G
5'
T
G
C
A
A
C
G
T
3'

Figure 3.

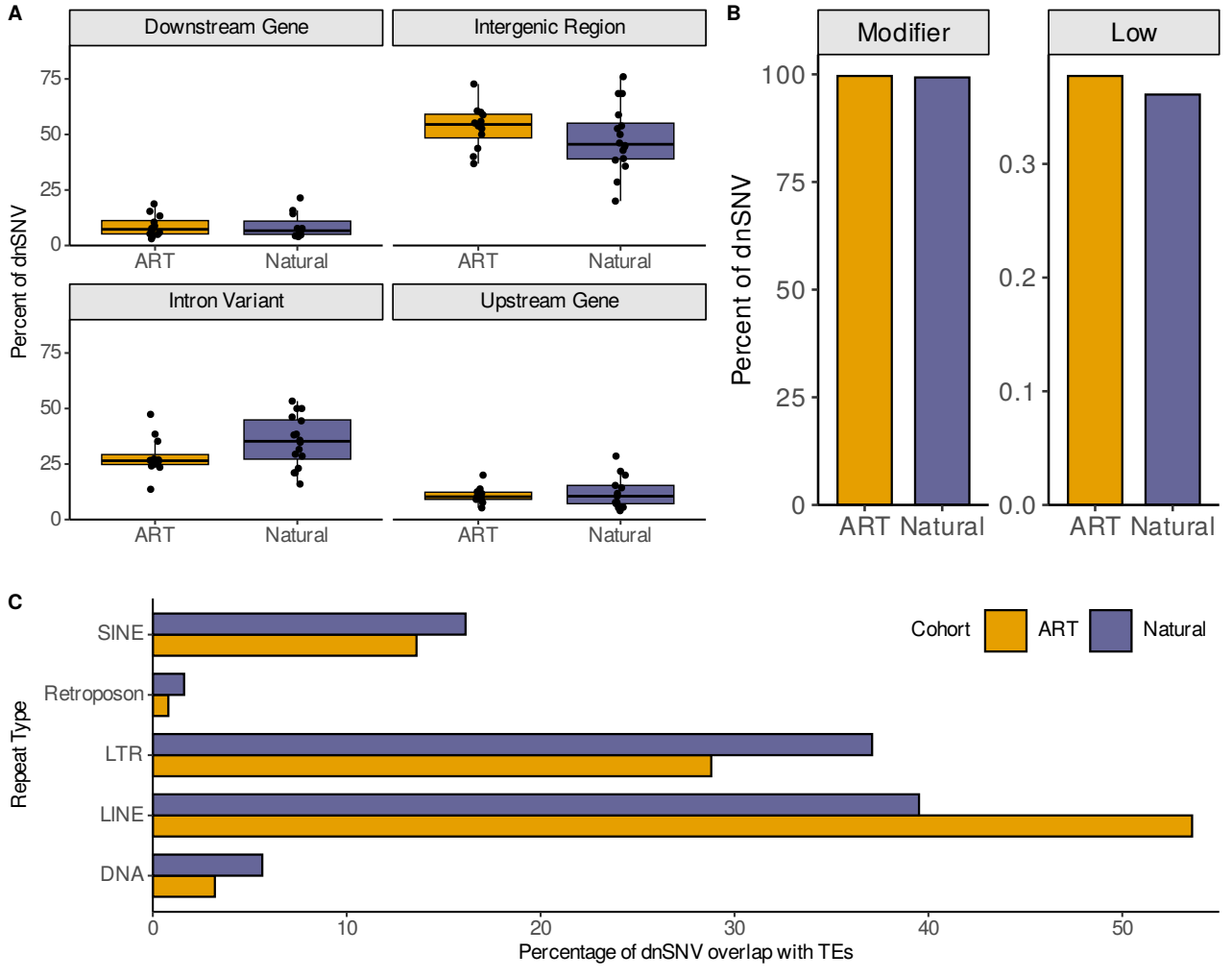
A
Downstream Gene
Intergenic Region
Intron Variant
Upstream Gene
Percent of dnSNV
0
25
50
75
ART
Natural
B
Modifier
Low
Percent of dnSNV
0
25
50
75
100
0.0
0.1
0.2
0.3
ART
Natural
C
Repeat Type
SINE
Retroposon
LTR
LINE
DNA
Cohort
ART
Natural
0
10
20
30
40
50
Percentage of dnSNV overlap with TEs